Supporting Information for

Novel targeted pH-responsive drug delivery system based on PEGMA modified bimetallic Prussian blue analogues for breast cancer chemotherapy

Qiang Chen[#1], Xiaoyu Huang[#2], Geyi Zhang[3], Jiangnan Li[1], Yang Liu[1], Xu Yan[1*]

1. Department of Orthopedics, The First Affiliated Hospital of Zhengzhou University, No. 1, Jianshe East Road, Zhengzhou 450052, P. R. China. Email: yanxu27@163.com
2. Department of Gastroenterology, The First Affiliated Hospital of Zhengzhou University, No. 1, Jianshe East Road, Zhengzhou 450052, P. R. China.
3. Department of Orthopedics, Yellow River Sanmenxia Affiliated Hospital of Henan University of Science and Technology, No. 2, Heping West Road, Sanmenxia 472000, P. R. China

[#]These authors contributed equally to this work.

S1. Experimental section

S1.1 Materials and chemicals

Cupric chloride ($CuCl_2 \cdot 2H_2O$), cobalt nitrate ($Co(NO_3)_2 \cdot 6H_2O$), potassium hexacyanocobaltate(III) ($K_3[Co(CN)_6]$) were purchased from Aladdin Chemical Reagent Co. Ltd. (Shanghai, China). N,N′-Methylenebisacrylamide (MBA, SIGMA Chemical Co., St. Louis, MO) and poly(ethylene glycol) methyl ether methacrylate (PEGMA , Aldrich). All reagents were of analytical grade, and all solutions were prepared with Milli-Q ultrapure water (≥18.2 MΩ·cm). Fetal bovine serum (FBS), phosphate buffer saline (PBS), Dulbecco's Modified Eagle Medium (DMEM), penicillin-streptomycin, trypsin-EDTA and Hoechst 33342 were purchased from Thermo Fisher Scientific. Cy3 labeled AS1411 was obtained from Scieworth, China. Doxorubicin (DOX), dimethyl sulfoxide (DMSO) and tetrazolium salt (MTT) were purchased from Sigma-Aldrich. Human breast cancer cell (MCF-7), mouse breast cancer cell (4T1) and normal mouse fibroblast (L929) were purchased from the Cell Bank of the Chinese Academy of Sciences (Shanghai, China).

S1.2 Preparation of solutions

Phosphate buffered saline (PBS, 0.01 M, pH 7.4) was prepared by mixing 0.242 g KH_2PO_4, 1.445 g $Na_2HPO_4 \cdot 12\ H_2O$, 0.2 g KCl, and 8.003 g NaCl. The stock solution of aptamer (50 nM), BLM and other interferences (10 $pg \cdot mL^{-1}$) were prepared using PBS and stored at 4 °C.

S1.3 Synthesis of CuFe PBA, CoFe PBA, CuFePBA@PEGMA and CoFePBA@PEGMA

CuFe PBA and CoFe PBA nanocubes were synthesized in accordance with previously described methods[1, 2]. Taking the preparation of CuFe PBA as an example, $CuCl_2 \cdot 2H_2O$ (127 mg) and polyvinylpyrrolidone (PVP, 3.0 g) were dissolved in deionized water (50 mL) under magnetic stirring to form solution **A**. $K_3[Fe(CN)_6]$ (82.5 mg) was also dissolved in 50 mL of Milli-Q water to form the transparent solution **B**. Then, the solution **B** was mixed with the solution **A** under agitated stirring. After 10 min, the reaction system was transferred and allowed to stand at room temperature for 24 h. Finally, the precipitate was washed three times with ethanol and then dried at 60 °C. As such, the CuFe PBA nanocubes were obtained. The preparation of the CoFe PBA nanocubes was similar with that of CuFe PBA except for replacing $CuCl_2 \cdot 2H_2O$ by $Co(NO_3)_2 \cdot 6H_2O$. The modification of PBA with PEGMA was carried out in accordance with the previous report [3].

S1.4 Basic characterizations

X-ray diffraction (XRD) patterns were obtained on a Rigaku D/Max-2500 X-ray diffractometer with Cu Kα radiation. X-ray photoelectron spectroscopy (XPS) was taken on a Thermo Fisher ESCALAB 250Xi photoelectron spectrometer. Fourier transform infrared spectrum (FT-IR) was recorded on a Bruker TENSOR 27 spectrometer (32 scans at 4 cm^{-1} resolution). Field emission scanning electron microscopy (FE-SEM) was taken on a JSM-6490LV scanning electron microscope. Transmission electron microscopy (TEM) was conducted on a JEOL JSM-6490L V system. Photoluminescence spectra of the samples were obtained using a fluorescence spectrophotometer (F-7000, Hitachi Ltd., Japan) with the excitation wavelength of

360 nm. UV-Vis spectra of the samples were recorded with a UV U3900 spectrophotometer (Hitachi Ltd., Japan) in the range of 200–800 nm. Cell cytotoxicity was quantified by measuring the absorbance at 490, using a microplate reader (Thermo Fisher Scientific, Inc., U.S.A.). Cellular uptake and intracellular distribution were studied using a confocal laser scanning microscopy (CLSM, LSM710, ZEISS, Germany). The sections for observing cellular ultrastructural distribution of nanoparticles were detected using a JEM-2100F high-resolution transmission electron microscope (HR-TEM, JEOL, Japan) operating at 120 kV. Ex vivo and in vivo imaging were performed at IVIS Lumina III system (PerkinElmer) with a suitable excitation/emission wavelength of 480/590 nm.

S1.5 Cytotoxicity Assays

Three different types of cell lines were used in the cytotoxicity assays, including human breast cancer cell (MCF-7), mouse breast cancer cell (4T1) and normal mouse fibroblast (L929). As for in vitro biocompatibility, the MTT assays were used to evaluate the cytotoxicity of CuFe PBA, CoFe PBA, CuFePBA@PEGMA and CoFePBA@PEGMA. Briefly, MCF-7, 4T1 and L929 cells were seeded in 96-well plates at 8×10^3 cells per well and incubated for 24 h at 37 °C and 5% CO_2. Different concentrations of CuFe PBA, CoFe PBA, CuFePBA@PEGMA and CoFePBA@PEGMA (5, 10, 20, 40, 80, and 160 μg mL^{-1}) were added and incubated for 24 h, separately. Then, the cells in each well were incubated for 48 h with fresh DMEM culture medium. Furthermore, after incubation with MTT (5 mg mL^{-1}, 20 μL) for 4 h, the plates were inverted to remove supernatant and 150 μL per well dimethyl

sulfoxide was added to dissolve the crystals remaining at the bottom of the plate. The absorbance was measured at 490 nm using a microplate reader (Thermo Fisher Scientific, Inc., U.S.A.). Cell viability was expressed as a percentage relative to untreated cells, which served as the control.

S2. Basic characterizations of all samples

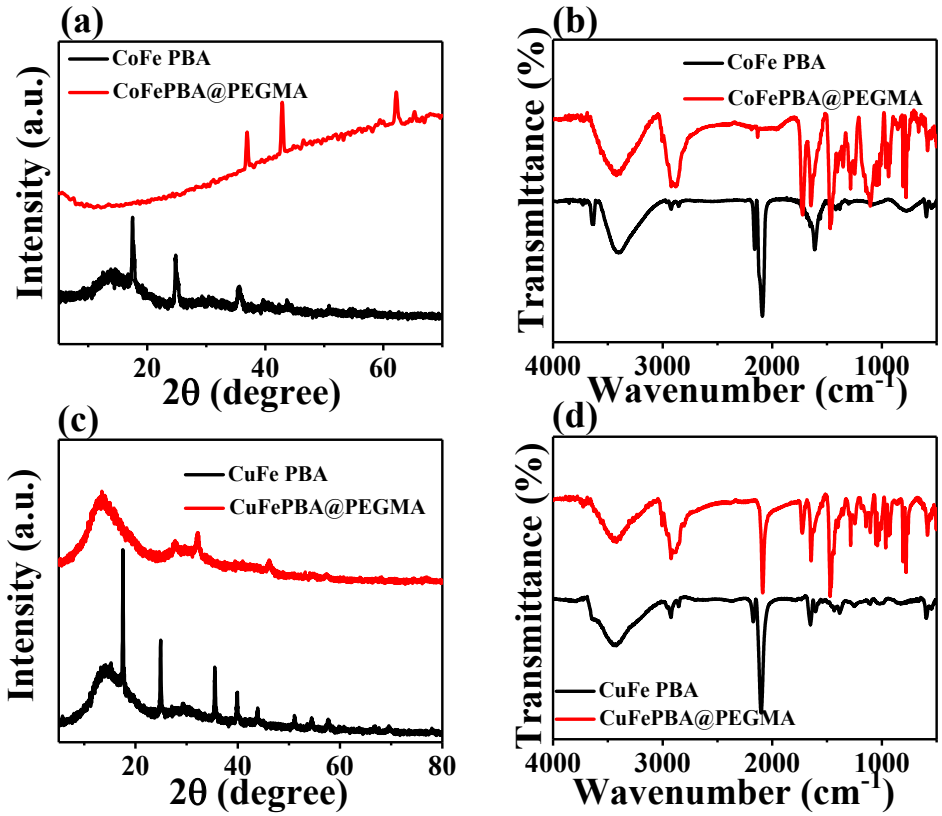

Fig. S1 (a, b) PXRD patterns and FT-IR spectra of (i) CoFe PBA and (ii) CoFePBA@PEGMA. (c, d) PXRD patterns and FT-IR spectra of (i) CuFe PBA and (ii) CuFePBA@PEGMA.

The chemical and crystal structures of pristine CoFe PBA and CoFePBA@PEGMA were characterized by powder X-ray diffraction (XRD), Fourier transform infrared spectroscopy (FT-IR), and Raman spectroscopy. As shown in **Fig. S1a**, the diffraction peaks of CoFe PBA at 17.6°,24.9°, 35.4°, 39.4 ° and 43.4° can be assigned to (200), (220), (400), (420) and (422) crystal planes of the $Co_3[Fe(CN)_6]_2$ (JCPDS No. 23-1089) with a face-centered-cubic structure, respectively. While the main crystal peaks disappeared after CuFe PBA modified with PEGMA, which may

be caused by the PEGMA cover up the pattern of the crystal. Moreover, the characteristic bands located at 2165, 2110, and 2098 cm^{-1} in the FT-IR spectrum of CoFe-PBA in the cyanide stretching region indicated to Co^{II}–NC–Fe^{III} (high spin), Co^{III}–NC–Fe^{II} (low spin) and Co^{II}–NC–Fe^{II} (reduced) sites, respectively [4]. However, these bands were absence in the FTIR spectra of CoFe PBA@PEGMA. Meanwhile, the broad band at ~3401 cm^{-1} belonged to the stretching vibration of O-H, while the band was shift to ~3414 cm^{-1} due to the stronger hydrogen bonds in the PEGMA. The results indicated that the PEGMA was covered on the prepared CoFe PBA successfully.

PXRD patterns collected at 300 K was indexed to the Prussian blue-like face centered cubic lattices in the space group Fmm (No. 225) (**Fig. S1c**). The characteristic peaks located at 17.7°, 25.2°, 35.7°, 40.4°, 44.3°, 51.9°, 55.3° and 58.3°, respectively, corresponded to the (200), (220), (400), (420), (422), (511), (440), (600) and (620) crystal planes of CuFe-PBA (JCPDS No. 02-0381). After modified with PEGMA, a broad the PXRD pattern of CuFe PBA@PEGMA ascribed to the PEGMA with the crystal pattern was weakened. Additionally, the FT-IR spectrum of the uncoated CuFe-PBA sample featured the characteristic bands at 2169 and 2102 cm^{-1} in the cyanide stretching region, due to Cu^{II}-NC-Fe^{III} and Co^{II}-NC-Fe^{II} sites, respectively [5]. Whereas the strong and broad absorption peak at 3700–3000 cm^{-1} was attributed to the O–H stretching vibration of CuFe-PBA. After modified with PEGMA, the O–H band was shifted from 3438 cm^{-1} to 3420 cm^{-1} for CuFePBA@PEGMA, indicating the presence of stronger hydrogen bonds between PEGMA and CuFe PBA [6].

The FT-IR spectrum of the CuFePBA@PEGMA composite showed a strong peak at 1466 cm^{-1} arising from the CH_2 group of PEGMA and the peak at 1100 cm^{-1} for C–O–C stretching of PEGMA, confirming the successful combination of PEGMA in the composite [7].

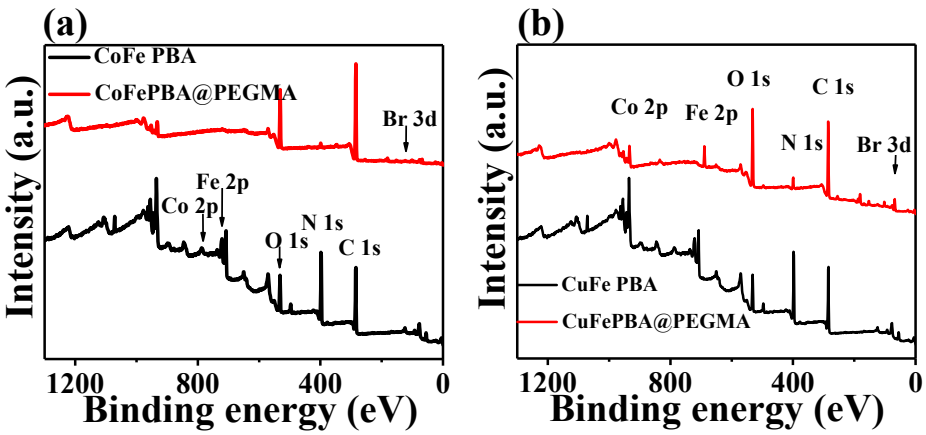

Fig. S2 (a) XPS survey spectra of (i) CoFe PBA and (ii) CoFePBA@PEGMA. (b) XPS survey spectra of (i) CuFe PBA and (ii) CuFePBA@PEGMA.

To verify the chemical structure and components of each element contained in CoFe PBA and CoFePBA@PEGMA, X-ray photoelectron spectroscopy (XPS) characterizations were also carried out. In **Fig. S2a**, the XPS survey spectra of two samples revealed the coexistence of Co, Fe, C, N and O in both CoFe PBA and CoFe PBA@PEGMA. The Co 2*p* and Fe 2*p* signals may be caused by the transition metals contained in the PBA nanobox, and the existence of C 1s and N 1s in the samples can be due to the -C≡N groups in $Co_3[Fe(CN)_6]_2$. Meanwhile, the Br signal was observed for the CoFe PBA@PEGMA owning to the initiator for PEGMA.

Moreover, XPS characterizations were applied to investigate chemical

components and environment of the prepared CuFe PBA and CuFePBA@PEGMA. The XPS survey spectra of CuFe PBA and CuFePBA@PEGMA are shown in **Fig. S2b** with C 1*s*, N 1*s*, Co 2*p* and Fe 2*p* peaks both appeared in the survey spectra of CuFePBA and CuFePBA@PEGMA. However, the N 1*s* XPS peak was weak, while the Br 3*d* peak was observed in CuFePBA@PEGMA.

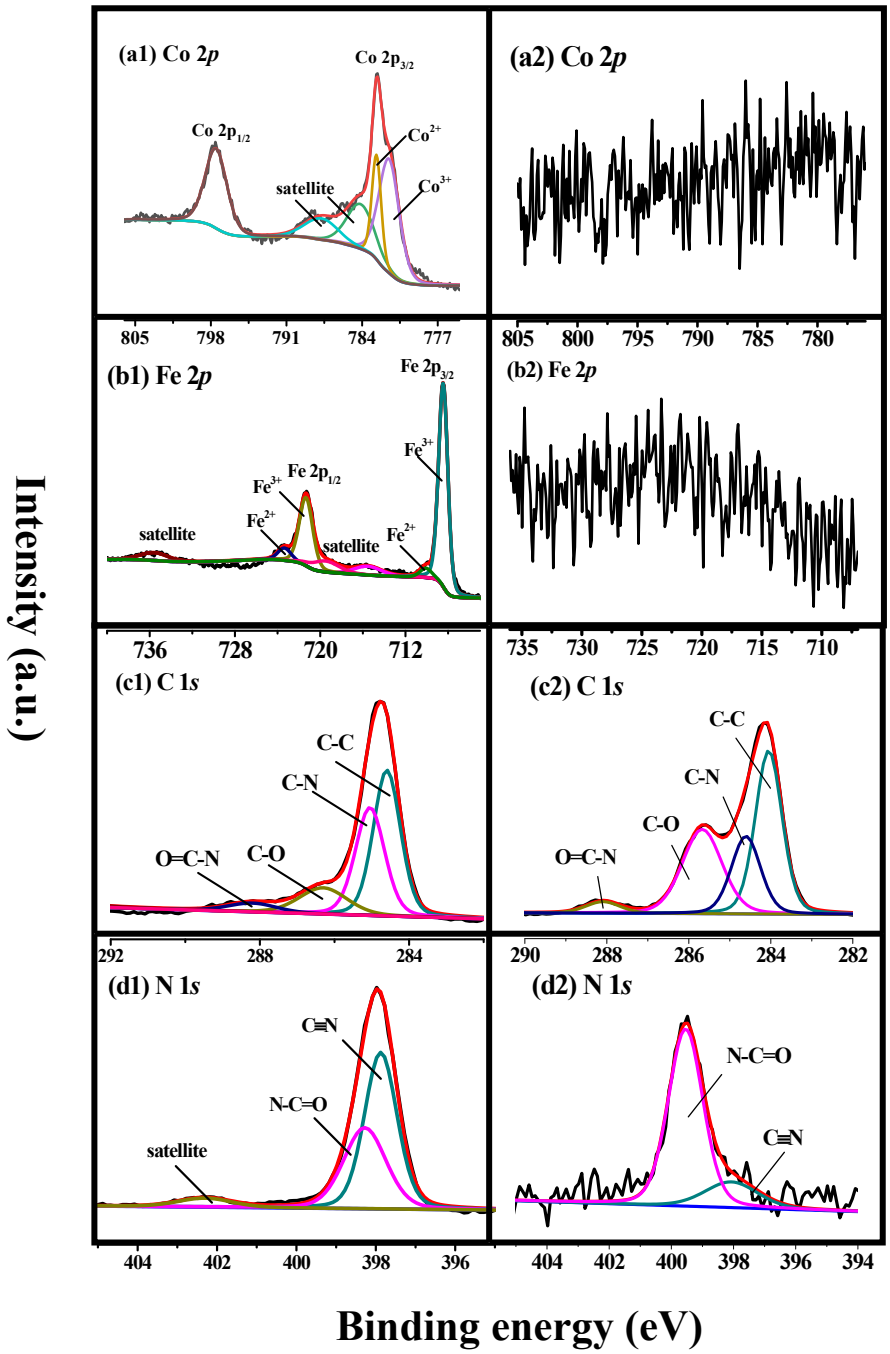

Fig. S3 High-resolution (a1-a2) Co 2*p*, (b1-b2) Fe 2*p*, (c1-c2) C 1s and (d1-d2) N 1*s* XPS spectra of CoFe PBA and CuFePBA@PEGMA, respectively.

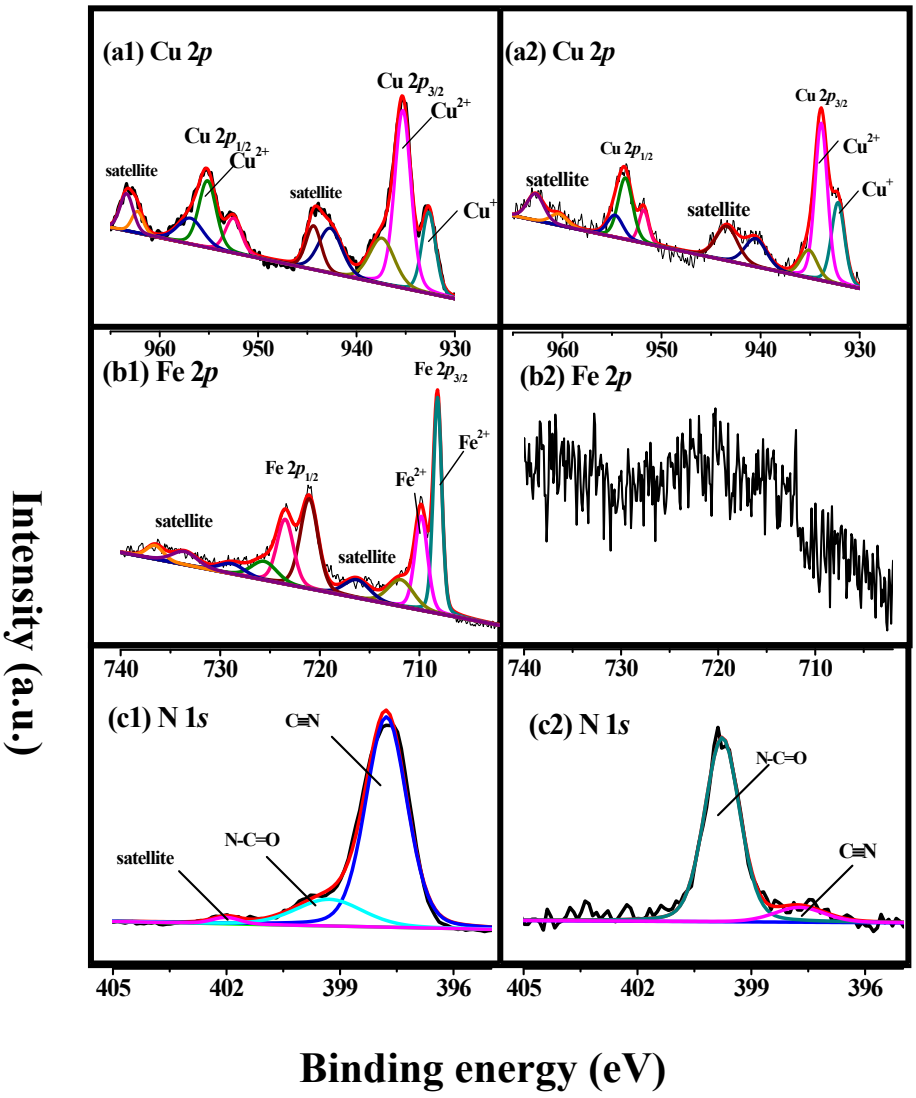

Fig. S4 The high-resolution (a) Cu 2*p*, (b) Fe 2*p*, (c) C 1*s*, and (d) N 1*s* XPS spectra of CuFe PBA and CuFePBA@PEGMA, respectively.

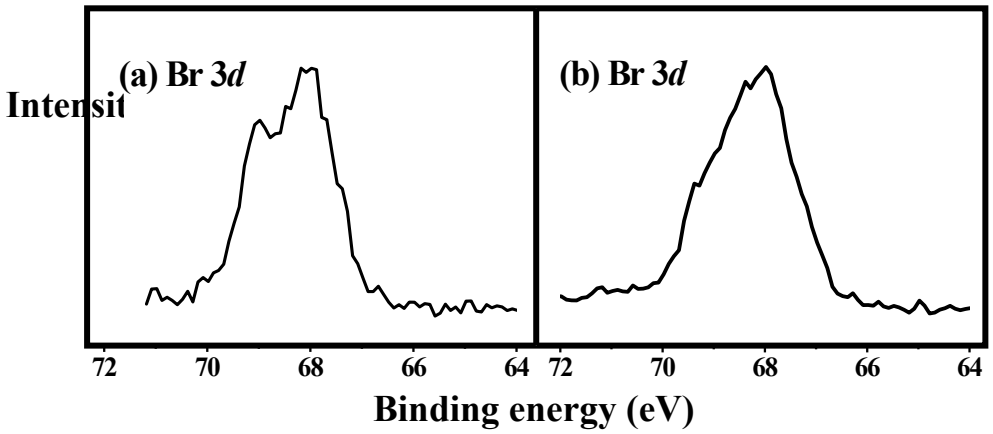

Fig. S5 High-resolution Br 3*d* XPS spectra of (a) CoFePBA@PEGMA and (b) CuFePBA@PEGMA

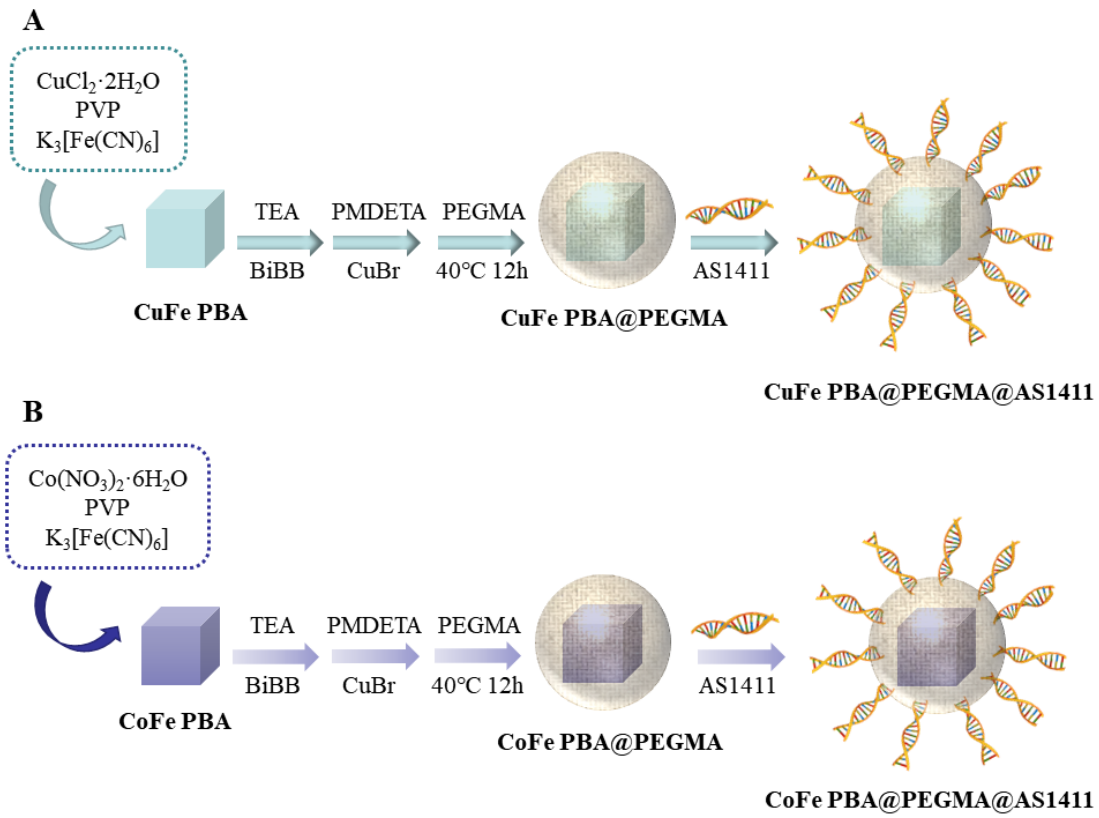

Fig. S6 Scheme of chemical structures and synthesis steps for CuFePBA@PEGMA@AS1411 (A) and CoFePBA@PEGMA@AS1411 (B).

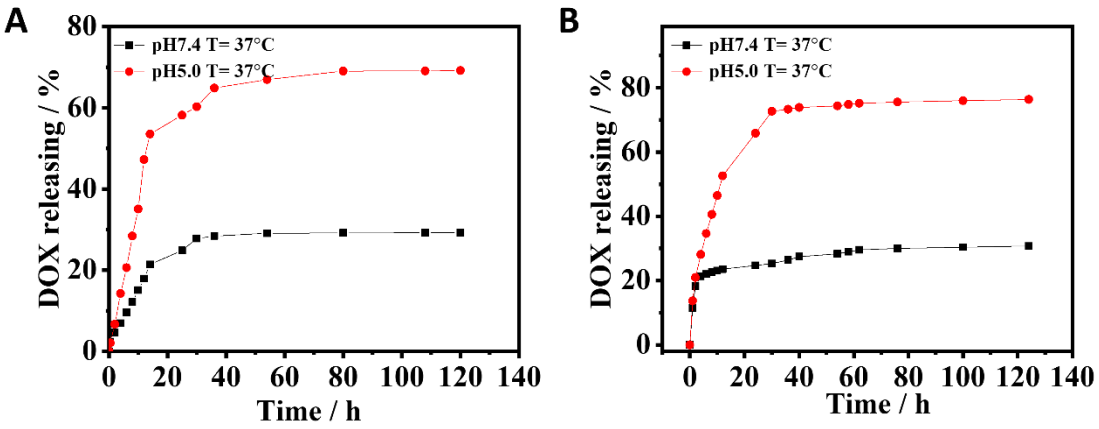

Fig. S7 The pH-dependent DOX release of CuFe PBA@PEGMA (A) and CoFe PBA@PEGMA (B)

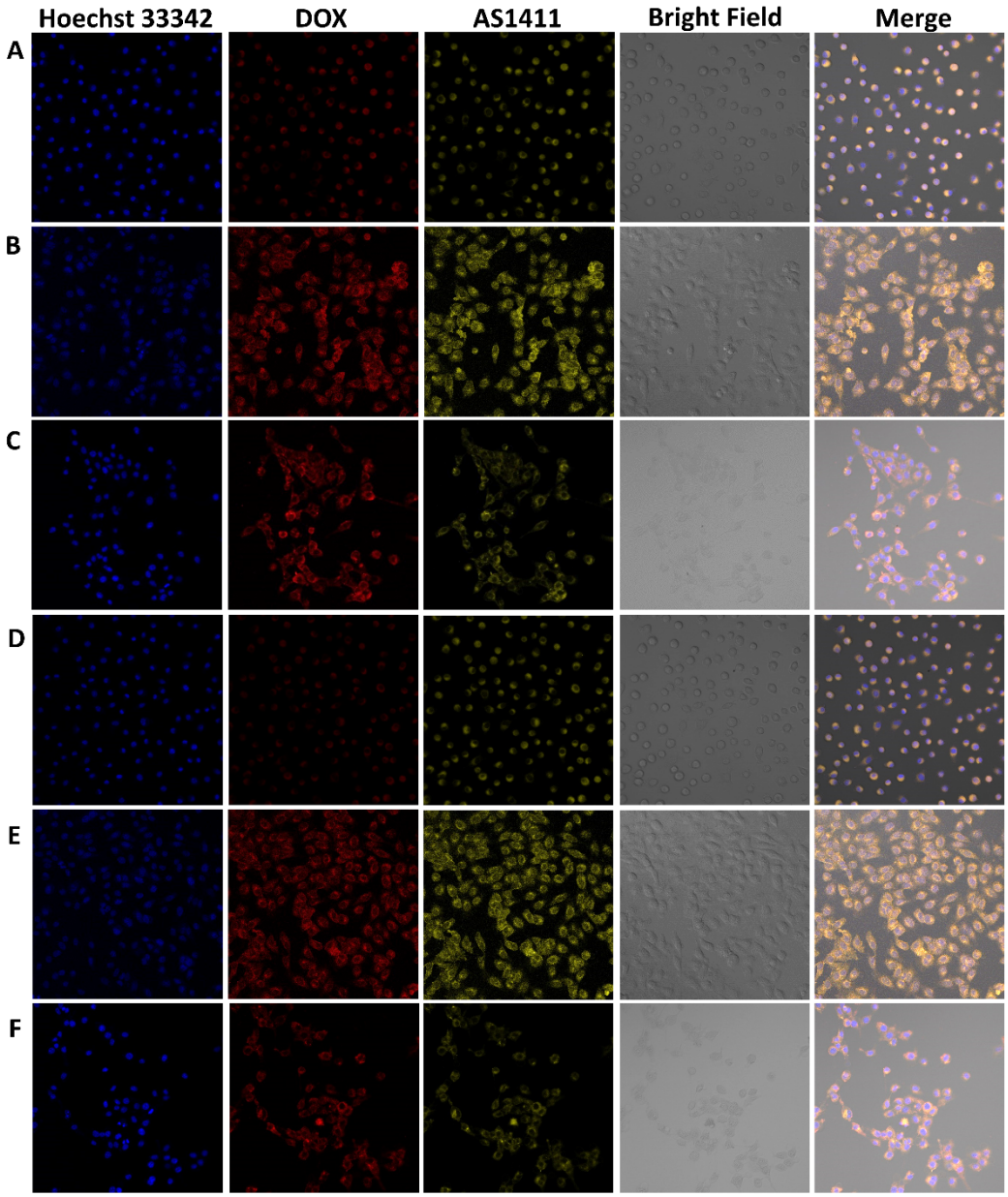

Fig. S8 Cellular uptake behaviors of CuFePBA@PEGMA@AS1411/DOX in L929 (A), MCF-7 (B), 4T1 cells (C) and CoFePBA@PEGMA@AS1411/DOX in L929 (D), MCF-7 (E), 4T1 cells (F) at pH=7.0 (The scale bar is 40 μm).

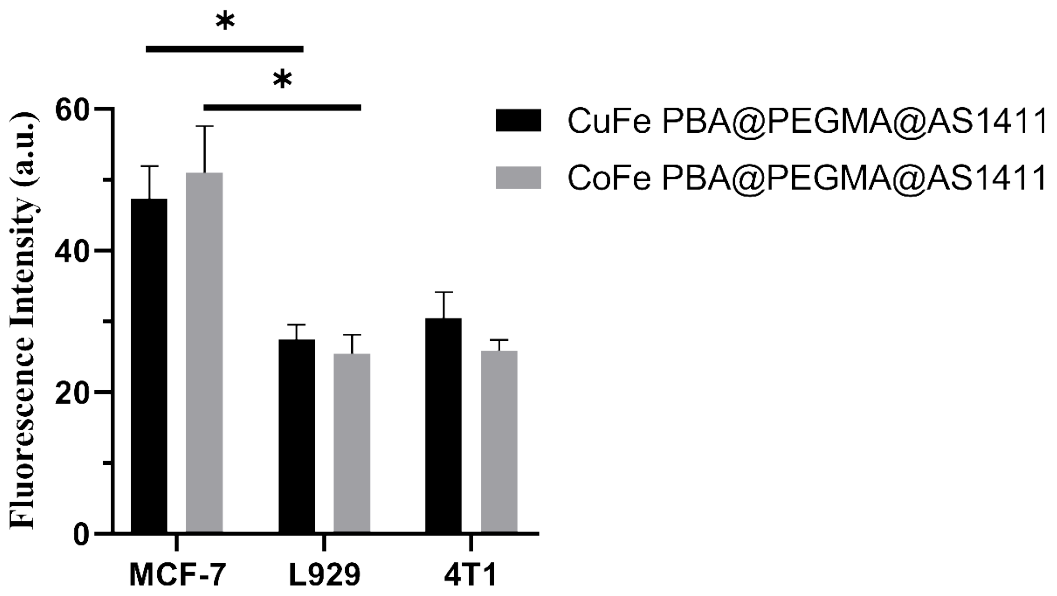

Fig. S9 The MFI analysis of AS1411 in MCF-7, L929 and 4T1 cells at pH=7.0. *P<0.05 vs L929 cells.

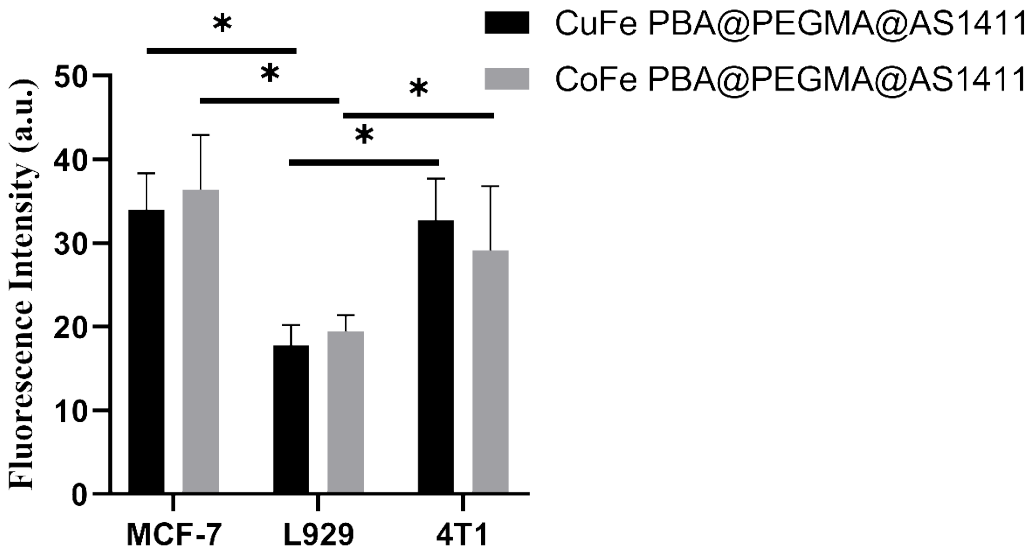

Fig. S10 The MFI analysis of DOX in MCF-7, L929 and 4T1 cells at pH=6.0. *P<0.05 vs L929 cells.

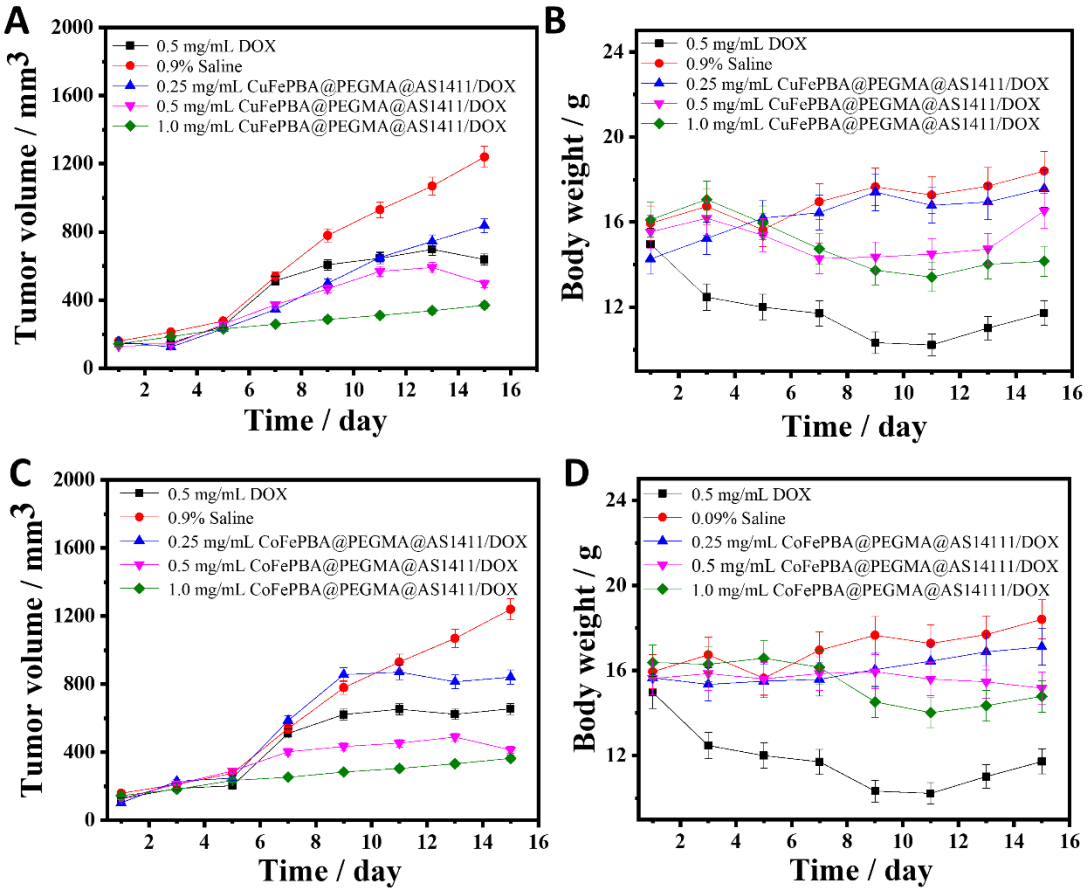

Fig. S11 In vivo anti-BC efficacy of CuFePBA@PEGMA@AS1411/DOX and CoFePBA@PEGMA@AS1411/DOX in 4T1 tumor-bearing mice. (A and C) The curves of tumor growth in mice with different treatments of 0.9% saline, 0.5 mg mL^{-1} DOX, 0.25, 0.5 and 1.0 mg mL^{-1} Nano-DOX; (B and D) Body weight curves of mice in the treating period.

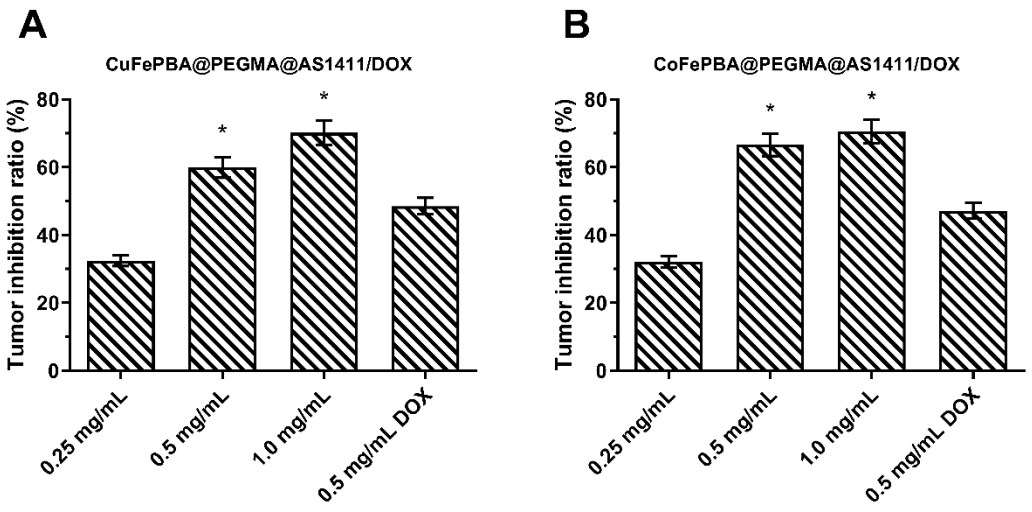

Fig. S12 The tumor inhibition rates of CuFePBA@PEGMA@AS1411/DOX and CoFePBA@PEGMA@AS1411/DOX in the 4T1 tumor-bearing mice. *P<0.05 vs DOX.

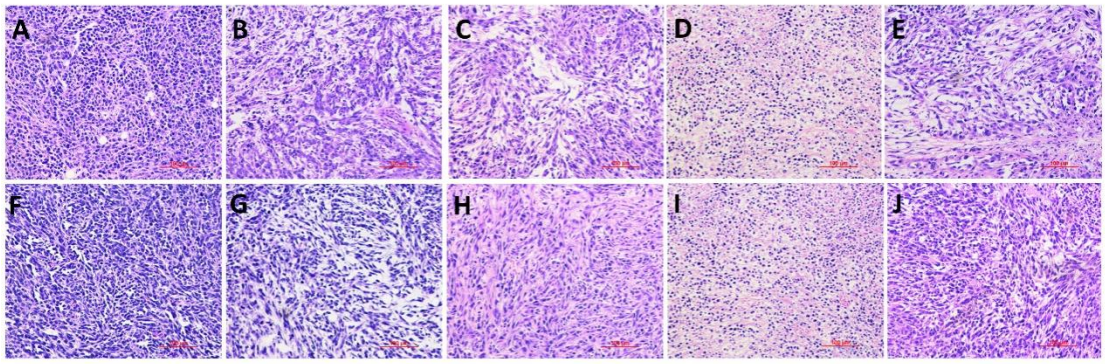

Fig. S13 Hematoxylin and eosin (H&E) staining of the tumor tissues after different treatments (A: 0.9% saline, B: 0.25 mg mL^{-1}, C: 0.5 mg mL^{-1}, D: 1.0 mg mL^{-1} CuFePBA@PEGMA@AS1411/DOX, E: 0.5 mg mL^{-1} DOX; F: 0.9% saline, G: 0.25 mg mL^{-1}, H: 0.5 mg mL^{-1}, I: 1.0 mg mL^{-1} CoFePBA@PEGMA@AS1411/DOX, J: 0.5 mg mL^{-1} DOX), scale bar = 100 μm.

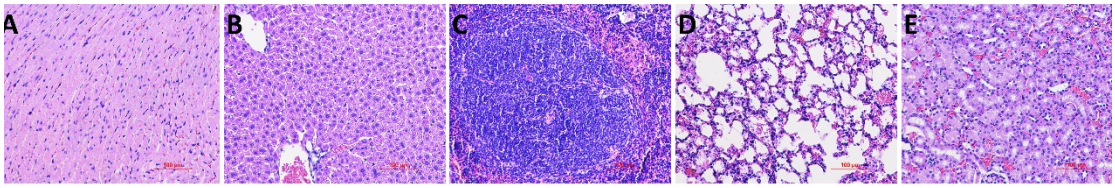

Fig. S14 The histological examination of vital organs from the healthy mice, including (A) heart, (B) liver, (C) spleen, (D) lung and (E) kidney. Scale bar = 100 μm.

Reference

1. Zhou, N., et al., *Core-Shell Heterostructured CuFe@FeFe Prussian Blue Analogue Coupling with Silver Nanoclusters via a One-Step Bioinspired Approach: Efficiently Nonlabeled Aptasensor for Detection of Bleomycin in Various Aqueous Environments.* Anal Chem, 2018. **90**(22): p. 13624-13631.
2. Gu, C., et al., *Multicomponent nanohybrids of nickel/ferric oxides and nickel cobaltate spinel derived from the MOF-on-MOF nanostructure as efficient scaffolds for sensitively determining insulin.* Anal Chim Acta, 2020. **1110**: p. 44-55.
3. Jia, Q.L., Z.; Guo, C.; Huang, X.; Kang, M.; Song, Y.; He, L.; Zhou, N.; Wang, M.; Zhang, Z.; Fu, G.; Du, M., *PEGMA-modified bimetallic NiCo Prussian blue analogue doped with Tb(III) ions: Efficiently pH-responsive and controlled release system for anticancer drug.* Chem Eng J, 2020. **389**: p. 124468.
4. Risset, O.N., et al., *Light Switchable Magnetism in a Coordination Polymer Heterostructure Combining the Magnetic Potassium Chromiumhexacyanochromate with the Light-Responsive Rubidium Cobalthexacyanoferrate.* Chem Mater, 2015. **27**(18): p. 6185-6188.
5. Asakura, D., et al., *Bimetallic Cyanide-Bridged Coordination Polymers as Lithium Ion Cathode Materials: Core@Shell Nanoparticles with Enhanced Cyclability.* J Am Chem Soc, 2013. **135**(7): p. 2793-2799.
6. Zhang, H., et al., *Structure and properties of maize starch processed with a combination of α-amylase and pullulanase.* Int J Biol Macromol, 2013. **52**: p. 38-44.
7. Jin, J., et al., *Fabrication of PP-g-PEGMA-g-heparin and its hemocompatibility: From protein adsorption to anticoagulant tendency.* Appl Surf Sci, 2012. **258**(15): p. 5841-5849.